Comparison of High Voltage and High Temperature Performances of Wide Bandgap Semiconductors for vertical Power Devices

Christophe Raynaud, Dominique Tournier, Hervé Morel, Dominique Planson

Comparison of High Voltage and High Temperature Performances of Wide Bandgap Semiconductors for vertical Power Devices

Christophe Raynaud, Dominique Tournier, Hervé Morel and Dominique Planson

Université de Lyon, CNRS, Laboratoire Ampère

INSA-Lyon, Ampere, UMR 5005, F-69621, France

Corresponding author: christophe.raynaud@insa-lyon.fr

ABSTRACT

Temperature dependant properties of wide band gap semiconductors have been used to calculate theoretical specific on-resistance, breakdown voltage, and thermal run away temperature in SiC, GaN and diamond, and Si vertical power devices for comparison. It appears mainly that diamond is interesting for high power devices for high temperature applications. At room temperature, diamond power devices should be superior to SiC only for voltage higher than 30-40 kV, due to the high energy activation of the dopants.

Keywords : wide bandgap, Power semiconductor devices, Semiconductor materials

1 INTRODUCTION

Progress in semiconductor technologies have been so consequent these last decades that theoretical limits of silicon, that have largely dominate the market, have been achieved. In the same time, research on other semiconductors, and especially wide band gap

semiconductors have allowed to realize a great variety of power devices : Schottky diodes, bipolar devices, MOSFET, JFET… [1] - [3]. Among these wide band gap materials, silicon carbide is the most advanced from a technological point of view: Schottky diodes are already commercially available and JFET will be soon. Due to their superior material properties, diamond and GaN should be even better than SiC. Applications for these wide band gap materials are high voltage devices but also high temperature devices.

In this paper, we have calculated theoretical characteristics such as breakdown voltage, taking into account multiplication of electrons, holes and multiplication in SCR, specific-on resistance, taking into account physical model of mobility when available in literature, maximum electric field, temperature of thermal runaway…for Silicon, Silicon carbide, GaN and diamond using an ideal planar semi infinite diode. Therefore the equations are resolved in the vertical direction only, with no edge effects. These results are compared with published experimental results and discussed.

2 DETAILS OF CALCULATIONS

2.1 PRELIMINARY CALCULATIONS

One important parameter for high voltage and high temperature capabilities of devices is the intrinsic carrier concentration n_i. The lower n_i is, the lower are leakage currents. Moreover, the temperature of thermal runaway of devices is defined as the temperature for which the intrinsic concentration becomes equal to the doping level of the active layer.

The intrinsic concentration n_i is calculated using the well-known formulas of semiconductors and taking into account the temperature (T) dependence of the semiconductor bandgap E_g as:

$E_g = E_g(300K) - \lambda(T - 300)$ for all SiC polytypes and diamond [4], [5], for values of λ, see Table I.

$$E_g = 3.28 - 7.7\times10^{-4}\frac{T^2}{(T+600)}$$ for 3C-GaN [6]

$$E_g = 3.47 - 7.7\times10^{-4}\frac{T^2}{(T+600)}$$ for 2H-GaN [6]

The effective density-of-state-mass for electrons is given by:

$$m_{dos,n} = (m_1 m_2 m_3)^{1/3}$$

and for holes :

$$m_{dos,p} = \left[m_{dp1}^{3/2} + m_{dp2}^{3/2} \cdot \exp\left(-\frac{\Delta_{so}}{kT}\right) + m_{dp3}^{3/2} \cdot \exp\left(-\frac{\Delta_{cf}}{kT}\right) \right]^{2/3}$$

k is Boltzmann constant, Δ_{so} is the spin-orbit splitting energy, and Δ_{cf} is the crystal-field splitting energy, m_{dpi} is the geometrical mean of the effective mass in longitudinal ($m_{\parallel}$) and transversal ($m_{\perp}$) direction in each of the 3 considered valence band (i = 1 for light holes, i = 2 for heavy holes and i = 3 for the split-off band), m_1, m_2 and m_3 are electron effective mass in the three main directions of the conduction band valley.

For silicon, we have used temperature dependence of bandgap [7] and effective density of state mass given in [8].

However, some of these fundamental parameters are not known in some of wide bandgap semiconductors, therefore Table I summarizes the parameters we have used.

Taking into account all these parameters, intrinsic concentrations have been calculated as a function of temperature and is plotted in Figure 1.

In regard to silicon, n_i is several decades lower in SiC or GaN band gap and further more lower in diamond, up to very high temperature. It is important to note that except for silicon the temperature dependence of effective mass is not known. Moreover, the temperature dependence of the bandgap for other semiconductors has not been demonstrated in a so widely range, so the high temperature values are an extrapolation. Finally, at temperature higher than 1000-1200 K, these semiconductors begin to be not very physically stable (for example, sublimation of silicon in SiC polytypes…).

2.2 THEORETICAL BREAKDOWN VOLTAGE

Main parameters to calculate the breakdown voltage and critical electric field are ionization coefficients of electrons and holes. According to the theoretical model of the lucky electron developed by Shockley [19], these coefficients are expressed as :

$$\alpha_{n,p} = a_{n,p} \cdot \exp\left(-\frac{b_{n,p}}{F}\right)$$

where F is the electric field in the structure, $a_{n,p}$ and b_{np} are constant but may depend on temperature. This formulation is in agreement with the empirical law of Chynoweth [20]. That is why this model is widely used for many semiconductors.
Table II summarizes retained values for ionization coefficients at room temperature. No temperature variations have been considered, due to a lack of data for the majority of these materials. However, the temperature dependence of breakdown voltage in Si [21] or in SiC [22] is not so high. It is important to note that only ionisation coefficient of holes in 6H and 4H-SiC have been determined in [23]. Values of electrons are obtained with the same ratio of 40 determined in 4H-SiC in [24]. In 3C-SiC, ionisation coefficients have been determined for holes and we assume that electron ionisation coefficients are the same [25]. For silicon, model of van Overstraeten – de Man have been used, as described in [26].

Using these coefficients, the multiplication coefficients in the p-type region M_p, in the n-type region M_n and in the space charge region MSCR are calculated using the following formula:

$$M_n = \frac{1}{1 - \int_{x_p}^{x_n} \alpha_n \cdot e^{-\int_{x_p}^{x} (\alpha_n - \alpha_p) dx}}$$

$$M_p = \frac{1}{1 - \int_{x_p}^{x_n} \alpha_p \cdot e^{\int_{x}^{x_n} (\alpha_n - \alpha_p) dx}}$$

$$M_{ZCE} = \frac{M_n \int_{x_p}^{x_n} qu \cdot e^{-\int_{x_p}^{x} (\alpha_n - \alpha_p) dx} \cdot dx}{\int_{x_p}^{x_n} qu \cdot dx}$$

The global multiplication factor is given by:

$$M = \frac{M_n J_n(x_p) + M_p J_p(x_n) + M_{ZCE} J_{SCR}}{J_{ph}(V_0)}$$

where $J_n(x_p)$, $J_p(x_p)$, J_{SCR} and $J_{ph}(V_0)$ are respectively the generated photocurrent density of electrons at the edge x_p of the P region, the generated photocurrent density of holes at the edge x_n of the N region, the generated photocurrent in the space charge region, and the dark current at zero bias. Their expressions are given in [28].

For a couple of values W_B, N_D of epilayer thickness and doping level, and for a given applied voltage, the electric field profile is calculated in the structure as a function of depth z. For each profile of F, the ionization coefficients, all previous ionization integrals and the multiplication factor M are calculated. Voltage is step by step incremented and value of V_{br} is considered when M is multiplied by 1000 between two steps of voltage. The maximum electric field F_c is the value of the electric field at the metallurgical junction for V_{br} when avalanche multiplication occurs. W_B is chosen so that the epilayer is not completely depleted even at breakdown (i.e. it is the case of a non punch through diode) so $W_B > W_{NPT}$.

Once the breakdown voltage and maximum electric field F_c have been calculated, the width of the non-punch through n-type diode W_{NPT} can be calculated with:

$$W_{NPT} = 2 \cdot \frac{V_{br}}{F_c} = \sqrt{\frac{2V_{br}}{q\varepsilon N_D}}$$

where ε is the dielectric permittivity of the semiconductor. That is the lower depth of the epilayer to block V_{br}, for a given doping level.

2.3 THEORETICAL SPECIFIC ON -RESISTANCE

After that, the specific on-resistance ρ_{on} (expressed in Ωcm²) is given by:

$$\rho_{on} = \rho W_{NPT}$$

where ρ is the bulk resistivity, depending on temperature and doping level of the material. The calculation of ρ needs to calculate the carrier drift mobility and the carrier concentration, which is not equal to the doping level due to the high activation energy of the dopants in wide band gap semiconductors. In Si, we assume that all dopants are ionized above room temperature.

So we need the activation energies (see Table III) of the commonly used dopants in each semiconductor. For n-type materials: nitrogen in 6H-SiC [29], [30] and 4H-SiC [31], Si in 2H-GaN [32], phosphorus in diamond [33]; for p-type materials aluminum in SiC [34] and boron in diamond [35].

Then the electron concentration is given by the resolution of the electroneutrality equation [36]. The electron drift mobility is the sum of contribution of the different scattering mechanisms – see [37], [38] for the complete description of the method - and can be calculated as a function of temperature and doping level for hexagonal silicon carbide. Because of a lack of theoretical data, electron mobility vs. doping level in 2H-GaN has been established by fitting experimental data of Ref. [39]. In the case of diamond, theoretical mobility has been calculated using data in Ref. [40] and Ref. [41]. For silicon, model of Masetti et al. [42] has been used for carrier mobility dependence. For cubic SiC, model of mobility described in Ref [43] has been used.

3 RESULTS ABOUT BREAKDOWN VOLTAGE

It is therefore possible to plot N_D vs. V_{br} (Figure 2) , F_c vs. N_D for the lower W value (Figure 3Figure) and also W_{NPT} vs. V_{br} (Figure 4).

As we can see from Figure 2 and Figure 3 the ionization coefficient used for diamond is obviously not appropriated because resulting V_{br} is lower than that expected from experimental results [44]. So in all next figures, data from [44] will be used for diamond.
Fit of curves from Figure 2 show that breakdown voltage as a function of doping level can be expressed as a power of N_D :

$$N_D = A_1 \cdot V_{br}^{-B_1}$$

where A_1 and B_1 are given in Table IV.
Fit of the curves from Figure 3 shows that the maximum electric field also varies as a power of the doping level following:

$$F_c = A_2 \cdot N_D^{B_2}$$

where A_2 and B_2 are given in Table V.
Fit of the curves from Figure 4 shows that the maximum electric field also varies as a power of the doping level following:

$$W_{NPT} = A_3 \cdot V_{br}^{B_3}$$

where A_3 and B_3 are given in Table VI.
Finally it is of interest to plot breakdown voltage as a function of the thermal runaway temperature at which the intrinsic carrier concentration becomes equal to the higher doping level that gives the considered breakdown voltage. This temperature is therefore higher in wider band gap materials, but is not dependent on the activation energy of dopants. This temperature is represented in Figure 5 as a function of breakdown voltage. Cubic and wurtzite GaN and wurtzite SiC are very close in terms of thermal limitation of blocking capabilities. Cubic SiC are able to support lower temperature but remains ~500°C above silicon. For diamond, parameters used shows no temperature limitation from the semiconductor (theoretical temperature ~1800°C) for V_{br} > 100 kV. However, precise ionization coefficients remain to be experimentally determined for diamond.
For wurtzite silicon carbide, ionization coefficients of holes have been found to decrease linearly with temperature between 250 and 550 K [23]. So our breakdown voltage values may be underestimated at high temperature. However, it is possible that Konstantinov ionization coefficients of electrons in 4H-SiC are underestimated [45].

4 RESULTS ABOUT FORWARD/REVERSE COMPARISON

Figure 6 and Figure 7 show the resulting ρ_{on} values as a function of breakdown voltage at 300 K and 600 K respectively. Values of ρ_{on} have been calculated with the same minimum width than at 300K, due to the temperature independent ionization coefficient that we have used. It is obvious that for a given V_{br}, the on-resistance is three orders of magnitude lower in SiC than in Si. This is due to the high maximum electric field that can be sustained by the material. Indeed it allows to reduce the epilayer width and so ρ_{on} for a given V_{br}.

Surprisingly, diamond R_{on}-V_{br} characteristic at room temperature is not superior to SiC or GaN ones. This is due to the very high activation energy of phosphorus (0.57 eV), which gives a very low concentration of carriers at room temperature. For example, at a

doping level of 10^{17} cm^{-3}, less than 0.03% of dopants are ionized at room temperature. But it can also be due to the relatively low electron mobility (1030 $cm^2V^{-1}s^{-1}$ at low doping level). This explains the difference with the results exposed by Saito et al. [46] who used an electron drift mobility of 3800 $cm^2V^{-1}s^{-1}$, without taking into account the incomplete ionization of dopants. So n-type diamond unipolar devices have no interest for applications with breakdown voltage lower than 50 kV at room temperature. On the contrary, at high temperature (600 K), due to the ionization of dopants, it is clear from Figure 7 than diamond becomes really superior to other semiconductors for voltage as low as ~1 kV. At 600 K, the specific on-resistance is increased by a factor 10 in silicon devices for V_{br} = 1 kV. 2H-GaN is very interesting, even superior to 4H-SiC, but its thermal conductivity is about 3 times lower than those of SiC. So that for high temperature applications, 4H-SiC remains more interesting.

For p-type diamond, due to the lower activation energy of boron (0.37 eV) than phosphorus in n-type, the ionization ration of dopants ~20 times higher in p-type than in n-type diamond. Assuming that hole mobility equals electron mobility, ρ_{on} should be ~20 times lower in p-type diamond.

Experimental results have been also reported on Figure 6 for comparison with theoretical results. Only devices without forward threshold voltage can be easily compared in terms of the on-state losses, i.e. bipolar transistors (BJT) [53], Junction Field Effect Transistors (JFET) [48] and SIT [50], MOSFET [49]. Other experimental devices such as Schottky diodes [51], and Junction Barrier diodes (JBS) [47] [55] have been plotted, but in these devices the on-state losses are not summed up in the dynamic on-state resistance. Bipolar devices such bipolar diodes or IGBT have not been summarized in this graph because in these devices, high minority carrier injection in forward bias allows to reduce the voltage drop due to the on-resistance in regards to device, so that comparing ρ_{on} have no sense.

Up to now, experimental results are always a little poorer than theoretical limits in SiC, that demonstrates that our estimations of theoretical limits are not so bad even with our incomplete knowledge of parameters. In GaN or diamond, theoretical limits will be probably translated towards lower on-resistance, and maybe towards higher breakdown values. There are surely larger evolution capabilities in GaN and diamond than in SiC now. The very high activation energies of dopants in diamond are a hard point to resolve. Some works have been done to decrease these activation energies for example with a deuteration treatment of boron doped diamond. Progress in the realization of ohmic contacts on n-type, in the etching of diamond will also lead to a decrease of the on-resistance and to the possibility of using quasi vertical structures. Relevant alternative ideas and concept are described in Ref. [58].

A heterojunction AlGaN/GaN Field Effect Transistor have been realized [56] and have achieved a breakdown voltage of 1600 V, with a specific on-resistance of 3.9 $m\Omega cm^2$, which is a good result in regards to the maturity of this material technology. Lateral Schottky rectifiers have shown V_{br} in the order of 6.5 kV together with a ρ_{on} = 0.2 $\Omega.cm^2$ [57].

For diamond, Schottky diodes have been realized with an exceptional breakdown voltage of 6.5 kV but with a very high specific on-resistance of 300 Ωcm^2 [44], that explained the representative point in out of range of the figure.

5 CONCLUSION

Numerical calculations of breakdown voltage, specific on-resistance and thermal run away temperature of unipolar devices have been presented, and compared with experimental published results. These calculations have been conducted taking into account the temperature dependence of physical properties of wide band gap materials, when they are known. It appears that i) published ionization coefficient in diamond are not in agreement with experimental results, ii) that p-type diamond becomes very interesting for high voltage devices at high temperature, at room temperature diamond is not superior to SiC for voltages less than 30-40 kV. In future, if the problem of n-type dopants in diamond can be resolved, then the on-resistance can be lowered and diamond will take advantages on the other materials. iii) that experimental results with 4H-SiC devices are not so far from theoretical limits. These limits could be refined by taking into account temperature dependence of ionization coefficients (not known except in Si and SiC), but also by resolving the heat equation. Then the on-losses could be properly evaluated by taking into account self-heating, and cooling systems. Moreover, thermal study of power devices should allow to compare vertical and lateral devices, that is a complicated challenge. This is the next step of this work.

6 REFERENCES

[1] T. P. Chow. Microelectronics Engineering, vol. 83 (2006) 112-122.

[2] R J. Trew, J.-B. Yan, and P. M. Mock. 1991 *Proc. IEEE*, vol. 79 n°5, (1991) 598-620,

[3] D. Stefani. Device Research. Conf., 2001, Notre Dame, In, USA. pp.14-16.

[4] G.L. Harris (Ed.), Properties of silicon carbide, INSPEC, The Institution of Electrical Engineers, London, 1995 (p.74).

[5] T. Watanabe, T. Teraji, T. Ito, Y. Kamakura and K. Taniguchi. " Monte Carlo simulations of electron transport properties of diamond in high electric fields using full band structures, " *J. Appl. Phys*., vol..95, n°9 (2004) 4866-4874.

[6] V. Bougrov, M. Levinshtein, S. Rumyantsev and A. Zubrilov, in *Properties of Advanced SemiconductorMaterials GaN, AlN, InN, BN, SiC, SiGe* . Eds. Levinshtein M.E., Rumyantsev S.L., Shur M.S., John Wiley & Sons, Inc., New York, 2001, pp. 1-30.

[7] W. Bludau and A. Onton. *J. Appl. Phys*., vol. 45, n°4 (1974) 1846-1848.

[8] R. Vankemmel, W. Schoenmaker and K. De Meyer. *Solid-State Electron*., vol. 36 n°10, (1993) 1379-1384.

[9] C. Persson and U. Lindefelt. *J. Appl. Phys*., vol. 82 n°11 (1997) 5496-5508.

[10] B. Rezaei , A. Asgari and M. Kalafi. *Physica B*, vol. 371 (2006) 107-111.

[11] M. Suzuki, T. Uenoyama and A. Yanase. *Phys. Rev. B*, vol. 52 n°11 (1995) 8132-8138.

[12] W. J. Fan, M. F. Li, T. C. Chong, and J. B. Xia. *J. Appl. Phys.*, vol. 79 n°1 (1996) 188-194.

[13] H. Kato, S. Yamasaki and H. Okushi. *Diamond & Rel. Mater*., vol. 16 (2007) 796-799.

[14] L. Reggiani, D. Waechter and S. Zutotynski. *Phys. Rev. B*, vol. 28 (1983) 3550-3554.

[15] L. Reggiani, S. Bosi, C. Canali, F. Nava and S. F. Kozlov. *Phys. Rev. B*, vol. 23 n°6 (1981) 3050-3056.

[16] W.J. Choyke and L. Patrick. *Phys. Rev.* , vol. 105 n°6 (1957) 1721-1723.
[17] R. Dalven. *J. Phys. Chem. Solids*, vol. 26 n°2 (1965) 439-441.
[18] V.S. Vavilov, and E. A. Konorova. *Sov. Phys. Usp*. vol., 19 n°4 (1976) 301-316.
[19] W. Shockley. *Solid-State Electron.*, vol. 2 n°1 (1961) 35-60.
[20] A.G. Chynoweth. *Phys. Rev*., vol. 109 n°5 (1958) 1537-1540.
[21] C.Y. Chang, S.S. Chiu, and L.P. Hsu. IEEE Trans. Electron Dev. vol. 18 n°6 (1971) 391-393.
[22] W.S. Loh, J.P.R. David, B.K. Ng, S. I. Soloviev, P.M. Sandvik, J. S. Ng1, and C.M. Johnson. "Temperature dependence of Hole Impact Ionization Coefficient in 4HSiC Photodiodes," presented at the ECSCRM'08 conference, Barcelona, Spain, Sept. 8–11, 2008, Paper MoP28.
[23] R. Raghunathan and B.J. Baliga. *Solid-State Electron*., vol. 43 n° 2 (1999) 199-211.
[24] A.O. Konstantinov, Q. Wahab, N. Nordell, and U. Lindefelt. *J. Electron. Mater*., vol. 27 n°4 (1998) 335-341.
[25] E. Bellotti, H.-E. Nilsson, K. F. Brennan, and P. P. Ruden. *J. Appl. Phys.*, vol. 85 n°6 (1999) 3211-3217.
[26] R.V. Overstraeten and H. de Man. *Solid-State Electron*., vol. 13 n°1 (1970) 583-608.
[27] I.H. Oguzman, E. Bellotti, K. F. Brennan, J. Kolnik, R. Wang, and P. P. Ruden. *J. Appl. Phys.*, vol. 81 n°12 (1997) 7827-7834.
[28] K. Isoird. "Study of high voltage abilities of Silicon Carbide power devices by OBIC and electrical measurements," Thesis, Ampere lab., INSA de Lyon, Lyon, France, 2001. In French.
[29] W. Suttrop, G. Pensl, W. J. Choyke, R. Stein, and S. Leibenzeder. *J. Appl. Phys*. vol. 72 n° 8 (1992) 3708-3713.
[30] C. Raynaud, F. Ducroquet, G. Guillot, L. M. Porter, and R. F. Davis. *J. Appl. Phys.*, vol. 76 n°3 (1994) 1956-1958.
[31] W. Götz, A. Schöner, G. Pensl, W. Suttrop, W. J. Choyke, R. Stein, and S. Leibenzeder. *J. Appl. Phys*., vol. 73 n° 7 (1993) 3332-3338.
[32] W. Götz, N.M. Johnson, C. Chen, H. Liu, C. Kuo, and W. Imler. *Appl. Phys. Lett.*, vol. 68 n° 22 (1996) 3144-3146.
[33] M. Katagiri, J. Isoya, S. Koizumi, and H. Kanda. *Appl. Phys. Lett.*, vol. 85 n° 26 (2004) 6365-6367.
[34] W. Suttrop, G. Pensl, and P. Lanig. *Appl. Phys. A.*, vol. 51 n° 3 (1990) 231-237.
[35] G. Sh. Gildenblat, S. A. Grot, and A. Badzian. *Proc. IEEE* **79**, 5 (1991) 647-668.
[36] J. Pernot, S. Contreras, J. Camassel, J. L. Robert, W. Zawadzki, E. Neyret, and L. Di Cioccio. *Appl. Phys. Lett.* vol.77 n° 26 (2000) 4359-4361.
[37] J. Pernot, W. Zawadzki, S. Contreras, J. L. Robert, E. Neyret, and L. Di Cioccio. *J. Appl. Phys.* vol. 90 n° 4 (2001) 1869-1878.
[38] C. Raynaud, "Propriétés physiques et électroniques du carbure de silicium," in *Technique de l'ingénieur*, D3-119, pp.1-14, 2007, in French.
[39] V. W. L. Chin, T. L. Tansley, and T. Osotchan. *J. Appl. Phys.* vol. 75 n° 11 (1994) 7365-7372.
[40] J. Pernot, C. Tavares, E. Gheeraert, E. Bustarret, M. Katagiri, and S. Koizumi. *Appl. Phys. Lett.* vol. 89 n° 12, (2006) 2111-2113.
[41] J. Pernot and S. Koizumi. *Appl. Phys. Lett.* vol. 93 n° 5, (2008) 052105.
[42] G. Masetti, M. Severi, S. Solmi. *IEEE Trans. Electron Dev.* vol. 30 n° 7 (1983) 764-769.
[43] M. Roschke and F. Schwierz. *IEEE Trans Electron Dev*, vol. 48 n° 7 (2001) 1442-1147.

[44] J. E. Butler, M. W. Geis, K. E. Krohn, J. Lawless Jr, S. Deneault, T. M. Lyszczarz, D. Flechtner, and R. Wright. *Semicond. Sci. Technol.*, vol.18 (2003) 67- 71.
[45] B.K. Ng, J. P. R. Dav id, R. C. Tozer, G. J. Rees, F. Yan, J. H. Zhao and M. Weiner. *IEEE Trans. Electron Dev.* vol. 50 n°8 (2003) 1724-1732.
[46] W. Saito, I. Omura, T. Ogura, and T. Ohashi. *Solid State Electronics*, vol. 48, (2004) 1555-1562.
[47] E.A. Imhoff and K.D. Hobart. Mater. Sci. Forum vols. 600-603 (2009) 943-946.
[48] L. Cheng, I. Sankin, V. Bondarenko, M.S. Mazzola, J.D. Scofield, D.C. Sheridan, P. Martin, J.R.B. Casady and J. B. Casady. Mater. Sci. Forum vols. 600-603 (2009) 1055-1058.
[49] M. Kitabatake, M. Tagome, S. Kazama, K. Yamashita, K. Hashimoto, K. Takahashi, O. Kusumoto, K. Utsunomiya, M. Hayashi, M. Uchida, R. Ikegami, C. Kudo and S. Hashimoto. Mater. Sci. Forum vols. 600-603 (2009) 913-918.
[50] Y. Tanaka, K. Yano, M. Okamoto, A. Takatsuka, K. Arai and T. Yatsuo. Mater. Sci. Forum vols. 600-603 (2009) 1071-1074.
[51] B. A. Hull, J. J. Sumakeris, M. J. O'Loughlin, Q. J. Zhang, J. Richmond, A. Powell, M. Paisley, V. Tsvetkov, A. Hefner and A. Rivera. Mater. Sci. Forum vols. 600-603 (2009) 931-934.
[52] A. Agarwal, A. Burk, R. Callanan, C. Capell, M. Das, S .Haney, B. Hull, C .Jonas, M. O'Laughlin, M. O'Neil, J. Palmour, A. Powell, J. Richmond, S.-H. Ryu, R. Stahlbush, J. Sumakeris and J. Zhang. Mater. Sci. Forum vols. 600-603 (2009) 895-900.
[53] H.S. Lee, M. Domeij, C.-M. Zetterling, R. Ghandi, M. Östling, F. Allerstam and E. O. Sveinbjörnsson. Mater. Sci. Forum vols. 600-603 (2009) 1151-1154.
[54] T. Yamamoto, J. Kojima, T. Endo, E. Okuno, T. Sakakibara and S. Onda. Mater. Sci. Forum vols. 600-603 (2009) 939-942.
[55] J. Hu, L.X. Li, P. Alexandrov, X. Wang and J. H. Zhao. Mater. Sci. Forum vols. 600-603 (2009) 947-950.
[56] Y.C. Choi, M. Pophristic, B. Peres, H.-Y. Cha, M.G. Spencer and L. F. Eastman. Semicond. Sci. Technol. 22 (2007) 517-521.
[57] A. P. Zhang, J. W. Johnson, F. Ren, J. Han, A. Y. Polyakov, N. B. Smirnov, A. V. Govorkov, J. M. Redwing, K. P. Lee, and S. J. Pearton. *App. Phys. Lett.*, vol. 78 n° 6 (2001) 823-825.
[58] CVD Diamond for Electronic Devices and Sensors. Edited by by Ricardo S. Sussmann, Wiley, 2009. 596p.

FIGURE CAPTIONS

Figure 1 : Intrinsic carrier concentration in various large bandgap semiconductor, displayed vs. reciprocal temperature.

Figure 2: Maximal doping level vs. theoretical breakdown voltage for several wide bandgap materials. Ref. is [44].

Figure 3: Maximum electric field vs. doping level for several wide bandgap materials. The position of the diamond curve is clearly false due to incorrect ionization coefficient.

Figure 4: Non punch through width vs. theoretical breakdown voltage for several wide band gap materials.

Figure 5: Run-away temperature as a function of breakdown voltage.

Figure 6: Theoretical resistance of the epilayer as a function of breakdown voltage at room temperature. Experimental results (stars) are extracted from [47] - [57] [44] [1]. Open square symbol represents an industrial component (JFET from SiCED).

Figure 7: Theoretical resistance of the epilayer as a function of breakdown voltage at 600 K.

FIGURE 1

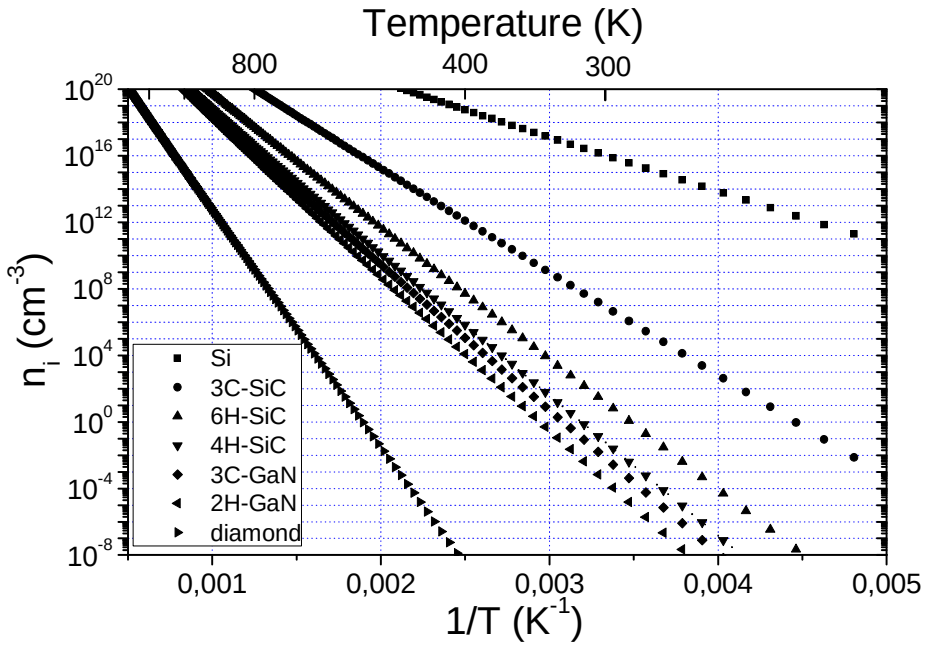
Temperature (K)
800
400
300
10^{20}
10^{16}
10^{12}
10^{8}
10^{4}
10^{0}
10^{-4}
10^{-8}
n_i (cm^{-3})
Si
3C-SiC
6H-SiC
4H-SiC
3C-GaN
2H-GaN
diamond
0,001
0,002
0,003
0,004
0,005
1/T (K^{-1})

FIGURE 2

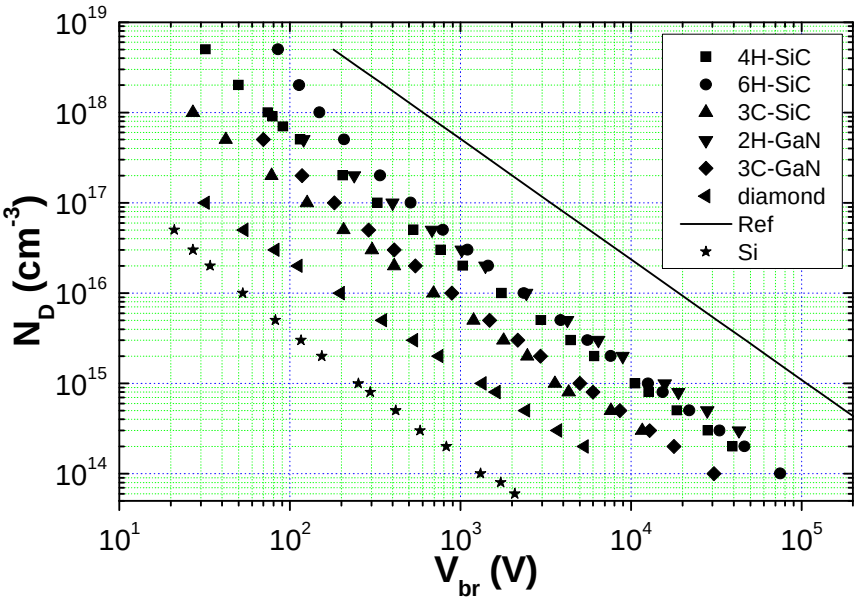
10^{19}
10^{18}
10^{17}
10^{16}
10^{15}
10^{14}
N_D (cm^{-3})
10^1
10^2
10^3
10^4
10^5
V_{br} (V)
4H-SiC
6H-SiC
3C-SiC
2H-GaN
3C-GaN
diamond
Ref
Si

FIGURE 3

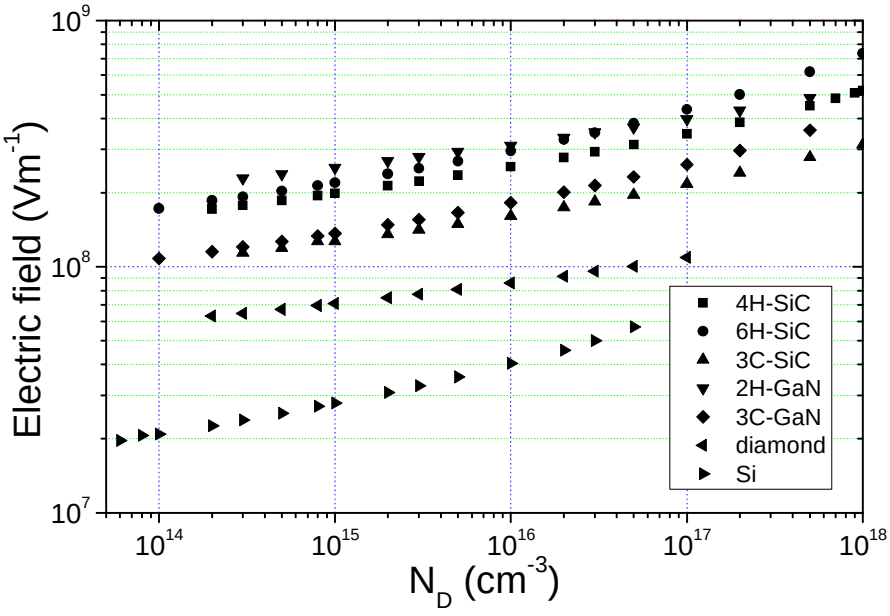
Electric field (Vm-1)
ND (cm-3)
4H-SiC
6H-SiC
3C-SiC
2H-GaN
3C-GaN
diamond
Si

FIGURE 4

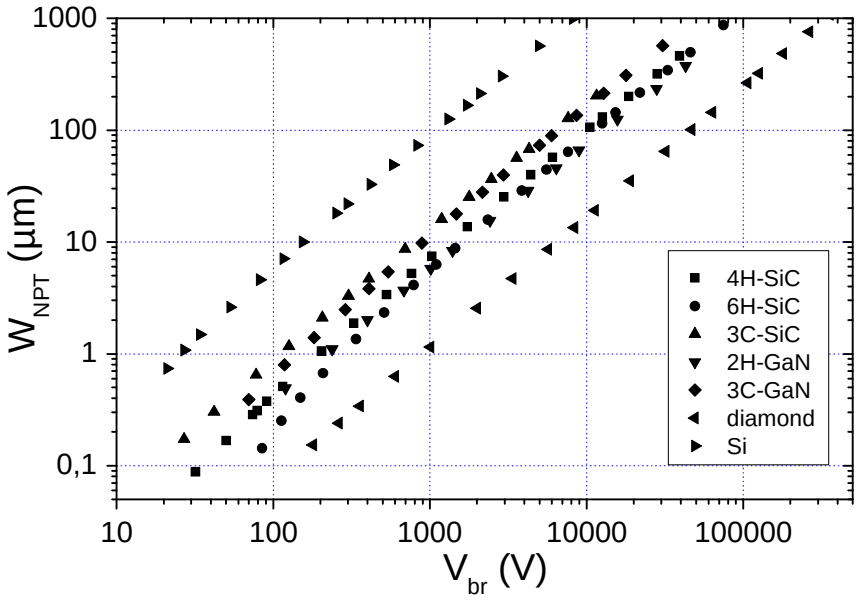
1000
100
10
1
0,1
W_{NPT} (µm)
10
100
1000
10000
100000
V_{br} (V)
4H-SiC
6H-SiC
3C-SiC
2H-GaN
3C-GaN
diamond
Si

FIGURE 5

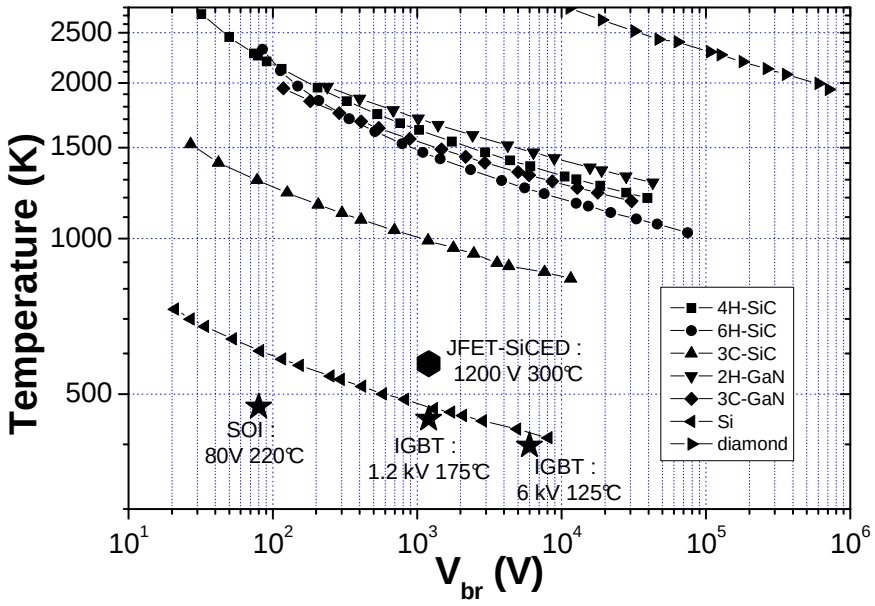
Temperature (K)
2500
2000
1500
1000
500
10^1
10^2
10^3
10^4
10^5
10^6
V_{br} (V)
4H-SiC
6H-SiC
3C-SiC
2H-GaN
3C-GaN
Si
diamond
JFET-SiCED :
1200 V 300℃
SOI :
80V 220℃
IGBT :
1.2 kV 175℃
IGBT :
6 kV 125℃

FIGURE 6

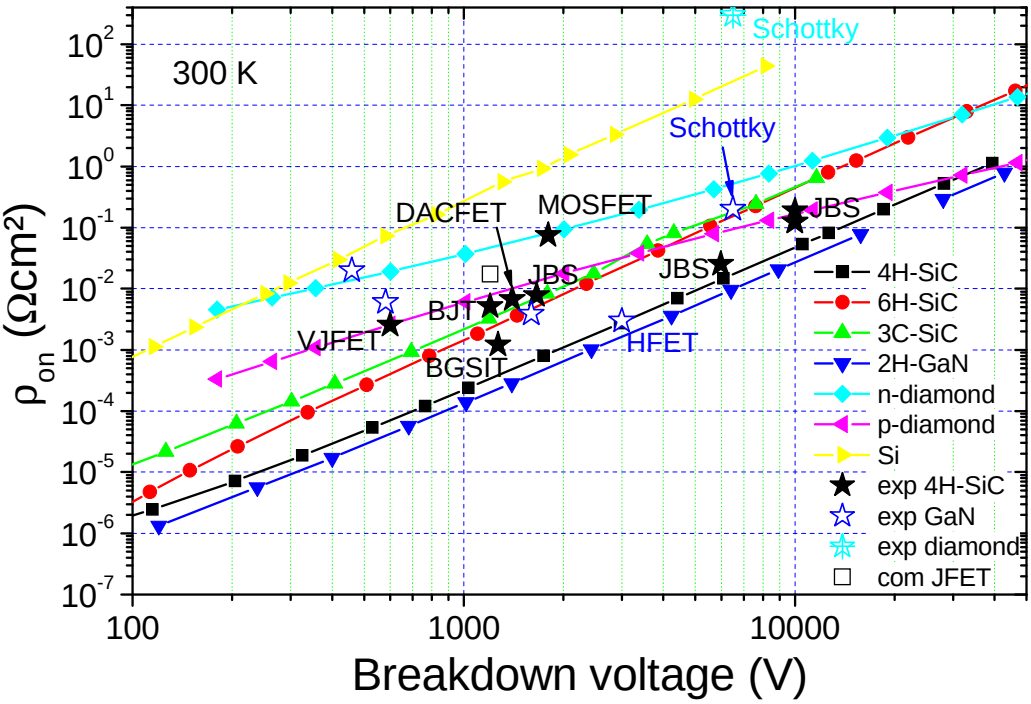
300 K
Schottky
Schottky
DACFET
MOSFET
JBS
JBS
JBS
BJT
VJFET
BGSIT
HFET
4H-SiC
6H-SiC
3C-SiC
2H-GaN
n-diamond
p-diamond
Si
exp 4H-SiC
exp GaN
exp diamond
com JFET
ρ_{on} (Ωcm²)
Breakdown voltage (V)
100
1000
10000
10^{2}
10^{1}
10^{0}
10^{-1}
10^{-2}
10^{-3}
10^{-4}
10^{-5}
10^{-6}
10^{-7}

FIGURE 7

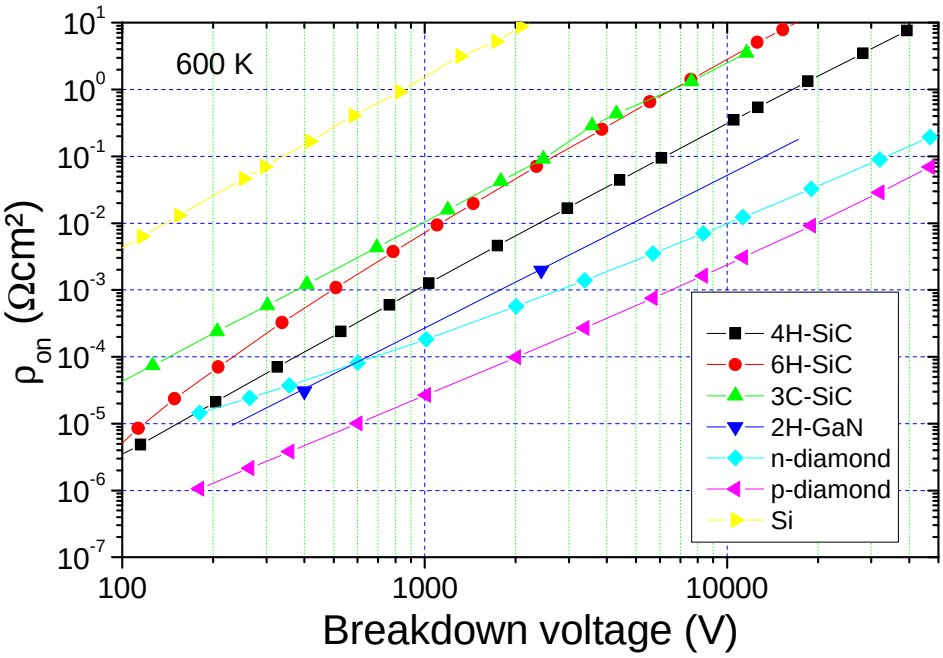
600 K
ρ_{on} (Ωcm^2)
Breakdown voltage (V)
100
1000
10000
10^{1}
10^{0}
10^{-1}
10^{-2}
10^{-3}
10^{-4}
10^{-5}
10^{-6}
10^{-7}
4H-SiC
6H-SiC
3C-SiC
2H-GaN
n-diamond
p-diamond
Si

TABLE I: Physical parameters for bandgap and effective mass temperature dependence in wide band semiconductors.

	6H-SiC	4H-SiC	3C-SiC	3C-GaN	2H-GaN	C
m_1/m_0	0.75 [9]	0.57 [9]	0.69 [9]	0.13 [10]	0.2 [6]	1.4 [13]
m_2/m_0	0.24 [9]	0.28 [9]	0.25 [9]	0.13 [10]	0.2 [6]	0.36 [13]
m_3/m_0	1.83 [9]	0.31 [9]	0.25 [9]	0.13 [10]	0.2 [6]	0.36 [13]
m_{dp1}/m_0	0.80 [9]	0.82 [9]	1.11 [9]	0.19 [12]	0.29 [11]	0.36 [14]
m_{dp2}/m_0	0.80 [9]	0.82 [9]	0.33 [9]	1.3 [12]	1.4 [11]	1.08 [14]
m_{dp3}/m_0	0.79 [9]	0.78 [9]	0.51 [9]	0.33 [12]	0.6 [11]	0.15 [14]
Δ_{so} (meV)	8.5 [9]	8.6 [9]	14.5 [9]	20 [6]	8 [11]	6 [15]
Δ_{cf} (meV)	53 [8]	72 [8]	0 [8]	0 [6]	40 [11]	0
Mc	6	3	3	1	1	6
$m_{dos,p}/m_0$	1.2	1.2	1.4	0.97	1.28	1.11
$m_{dos,n}/m_0$	0.69	0.37	0.35	0.13	0.2	0.57
Eg(300K) (eV)	2.925 [4]	3,165 [4]	2,2 [4]	3,203 [6]	3,393 [6]	5.47 [5]
λ ($eV°K^{-1}$)	$3{,}3\times10^{-4}$ [16]	$3{,}3\times10^{-4}$	$5{,}8\times10^{-4}$ [17]			$5{,}4\times10^{-5}$ [18]

m_0 is the free electron mass. H is denomination of silicon carbide or GaN is related to the hexagonal structure of the material (wurtzite crystallographic structure), C is related to the cubic structure of the material (zinc blend crystallographic structure).

TABLE II: Ionization coefficients for electrons and holes at room temperature for different wide band gap semiconductors.

	electrons		holes	
	a_n (cm^{-1})	b_n (Vcm^{-1})	a_p(cm^{-1})	b_p (Vcm^{-1})
4H-SiC [24]	4.1×10^5	$1{,}67\times10^7$	$1{,}63\times10^7$	$1{,}67\times10^7$
6H-SiC [23]	6.5×10^4	$1{,}5\times10^7$	$2{,}6\times10^6$	$1{,}5\times10^7$
3C-SiC [25]	1.07×10^7	1.12×10^7	1.07×10^7	1.12×10^7
3C-GaN [27]	4.68×10^8	1.23×10^7	1.03×10^6	8.22×10^6
2H-GaN [27]	2.9×10^8	3.44×10^7	4.81×10^6	1.94×10^7
Diamond [2]	1.935×10^8	7.749×10^6	1.935×10^8	7.749×10^6

TABLE III : Activation energies of main commonly used dopants in wide band gap semiconductors.

	4H-SiC	6H-SiC	2H-GaN	diamond
Donors (E_d=)	0.059 eV 0.102 eV	0.082 eV 0.14 eV	0.017 eV	0.57 eV
Acceptors (E_a =)	0.19 eV	0.2 eV 0.22 eV **	0.2 eV*	0.37 eV

* assumed value. ** we assume that Al occupies the two different lattices sites in 6H-SiC.

TABLE IV : Theoretical values of A_1 and B_1, according to the previous formula, in which V_{br} is expressed in V, and N_D in cm-3.

	A_1	B_1
4H-SiC	3.77×10^{20}	1.389
6H-SiC	1.76×10^{21}	1.519
3C-SiC	6.98×10^{19}	1.344
2H-GaN	1.88×10^{20}	1.257
3C-GaN	1.31×10^{20}	1.379
Si	2.67×10^{18}	1.405

TABLE V: Theoretical values of A_2 and B_2, according to the previous formula, in which F_c is expressed in Vm^{-1}, and N_D in cm^{-3}.

	A_2	B_2
4H-SiC	1.66×10^{6}	0.138
6H-SiC	6.14×10^{5}	0.170
3C-SiC	1.87×10^{6}	0.122
2H-GaN	7.94×10^{6}	0.100
3C-GaN	1.21×10^{6}	0.137
Si	2.08×10^{5}	0.143

TABLE VI : Theoretical values of A_3 and B_3, according to the previous formula, in which W_{NPT} is expressed in µm, and V_{br} in V.

	A_3	B_3
4H-SiC	1.75×10^{-3}	1.19
6H-SiC	8.17×10^{-4}	1.25
3C-SiC	4.09×10^{-3}	1.16
2H-GaN	2.35×10^{-3}	1.13
3C-GaN	2.88×10^{-3}	1.19
Si	2.22×10^{-2}	1.20
diamond	3.55×10^{-4}	1.167